Prevalence of strong bottom currents in the greater Agulhas system

Meghan F. Cronin,[1] Tomoki Tozuka,[2] Arne Biastoch,[3] Jonathan V. Durgadoo,[3] and Lisa M. Beal[4]

Received 20 February 2013; revised 19 March 2013; accepted 20 March 2013; published 10 May 2013.

[1] Deep current meter data and output from two high-resolution global ocean circulation models are used to determine the prevalence and location of strong bottom currents in the greater Agulhas Current system. The two models and current meter data are remarkably consistent, showing that benthic storms, with bottom currents greater than $0.2\,m\,s^{-1}$, occur throughout the Agulhas retroflection region south of Africa more than 20% of the time. Furthermore, beneath the mean Agulhas Current core and the retroflection front, bottom currents exceed $0.2\,m\,s^{-1}$ more than 50% of the time, while away from strong surface currents, bottom currents rarely exceed $0.2\,m\,s^{-1}$. Implications for sediment transport are discussed and the results are compared to atmospheric storms. Benthic storms of this strength ($0.2\,m\,s^{-1}$) are comparable to a $9\,m\,s^{-1}$ (Beaufort 5) windstorm, but scaling shows that benthic storms may be less effective at lifting and transporting sediment than dust storms. **Citation:** Cronin, M. F., T. Tozuka, A. Biastoch, J. V. Durgadoo, and L. M. Beal (2013), Prevalence of strong bottom currents in the greater Agulhas system, *Geophys. Res. Lett.*, *40*, 1772–1776, doi:10.1002/grl.50400.

1. Introduction

[2] While the mean ocean circulation can be thought of as wind-driven gyres in the upper ocean and creeping thermohaline flow in the deep ocean, strong currents and benthic storms do occur at the bottom of the ocean, particularly beneath strong surface currents such as found in western boundary regions [*Arbic et al*., 2009; *Savidge and Bane*, 1999; *Kontar and Sokov*, 1997]. In this study, we investigate the prevalence of strong bottom currents in the greater Agulhas system, where the western boundary current of the South Indian Ocean gyre, the Agulhas Current, flows past the African landmass terminus and retroflects to become the eastward flowing Agulhas Return Current (ARC).

[3] Strong bottom currents have important dynamical and practical implications. Prevailing winds can cause a buildup of energy within the ocean that must be dissipated in order to maintain global energy balance [*Ferrari and Wunsch*, 2009]. Because dissipation scales as velocity cubed, strong benthic currents are very effective at dissipating this energy. Strong bottom currents can also affect the topography of the seafloor by lifting and transporting sediment and organic matter off the seabed and by affecting the sedimentation rate of detritus raining down from above. Sediment layers thus provide a record of the paleo-climate and bottom currents extending back millions of years [*Schlüter and Uenzelmann-Neben*, 2007]. Furthermore, implementation plans for observing the deep ocean [*Garzoli et al*., 2010] and its sediment bed [*Zahn et al*., 2010] depend upon the range of current speeds that might be encountered at the bottom of the ocean.

[4] We use the term "benthic storm" here to refer to any strong bottom current event, except those that occur more than 50% of the time and are unidirectional. These are associated with a bottom "mean jet." Energetic currents at the bottom of the ocean have been linked to a number of processes: to the barotropic component of a surface jet (particularly for western boundary currents flowing poleward along a shallow continental slope) [*Beal and Bryden*, 1999], instabilities on the upper ocean jet [*Cronin and Watts*, 1996], form drag associated with variability in the thermocline [*Hogg*, 1983], topographic Rossby waves [*Thompson and Luyten*, 1976], and a spectrum of processes near seamounts [*Lavelle and Mohn*, 2010]. On shorter time scales, deep flow can be associated with near-inertial waves that are generated at the surface and propagate into the deep ocean [*Park et al*., 2010], and with tides. Benthic storms have been observed beneath meanders within nearly all strong current systems, including the Gulf Stream, where bottom currents reach more than $0.4\,m\,s^{-1}$ [*Savidge and Bane*, 1999], and the Antarctic Circumpolar Current as it flows through Drake Passage, where bottom currents reach more than $0.6\,m\,s^{-1}$ [*Chereskin et al*., 2009]. We expect the Agulhas system's strong surface currents, rich eddy field, and large topographic relief [*Beal et al*., 2011; *Biastoch et al*., 2008; *Boebel et al*., 2003] combine to make for potentially a very energetic bottom flow field. In this study, we use current meter data augmented with output from two high-resolution ocean general circulation models (OGCMs) to investigate the prevalence of strong bottom currents in the greater Agulhas system. By doing this analysis on two different OGCMs, in conjunction with in situ observations, we are able to illustrate robustness in our results.

2. Methodology and Data

[5] Previous studies of the bottom flow field have generally focused on the mean of the flow, its eddy kinetic energy [*Scott et al*., 2010], and the cubic bottom speed [*Arbic et al*.,

All Supporting Information may be found in the online version of this article.

[1]NOAA Pacific Marine Environmental Laboratory, Seattle, Washington, USA.
[2]Department of Earth and Planetary Science, Graduate School of Science, University of Tokyo, Tokyo, Japan.
[3]GEOMAR Helmholtz Centre for Ocean Research Kiel, Kiel, Germany.
[4]Rosenstiel School of Marine and Atmospheric Sciences, University of Miami, Miami, Florida, USA.

Corresponding author: M. F. Cronin, NOAA Pacific Marine Environmental Laboratory, 7600 Sandpoint Way NE, Seattle, WA 98115, USA. (Meghan.F.Cronin@noaa.gov)

0094-8276/13/10.1002/grl.50400

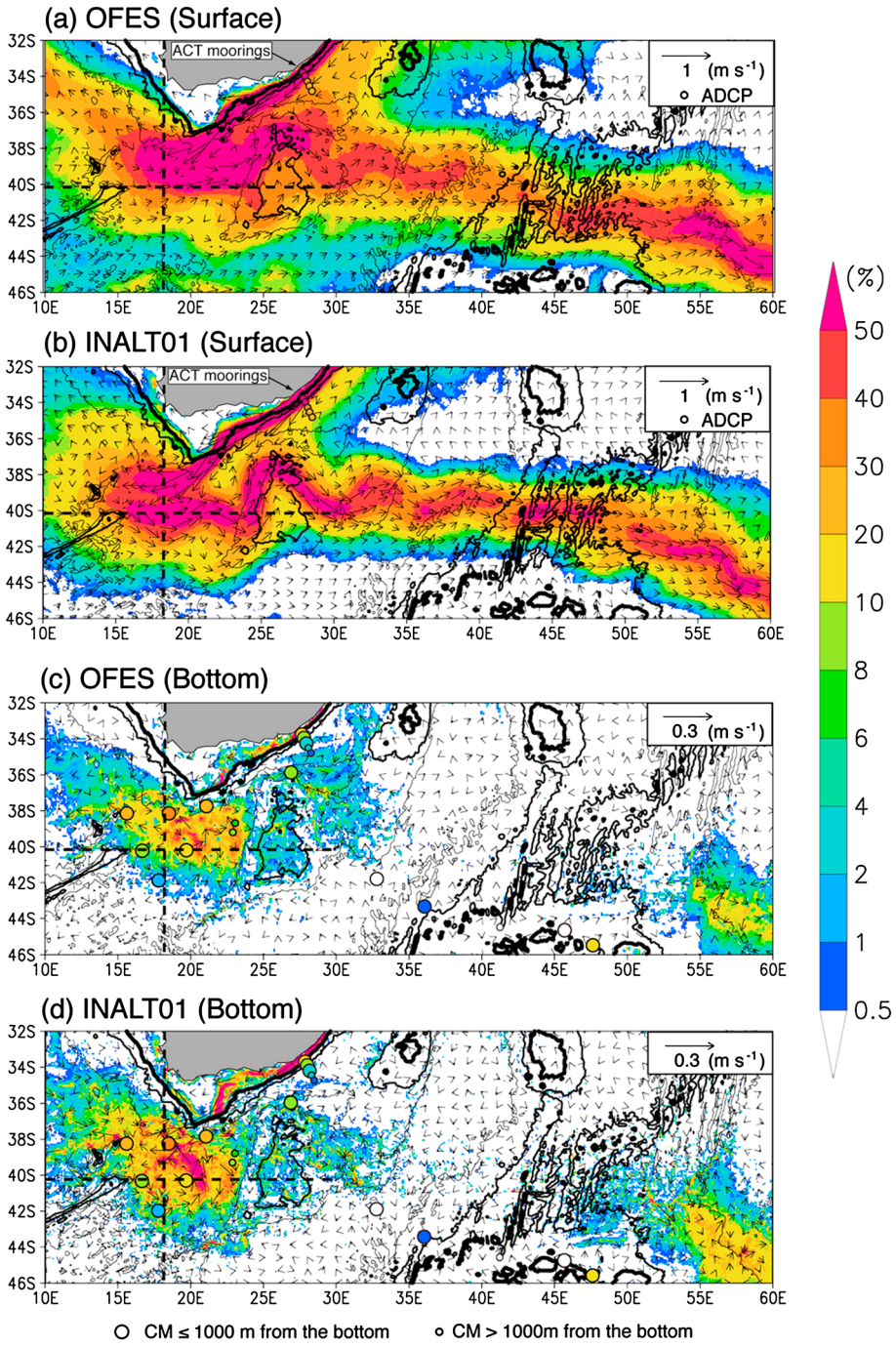

Figure 1. Map of percentage of record with currents greater than threshold values (a and b) for surface currents $>0.5\,\mathrm{m\,s^{-1}}$ and (c and d) for bottom currents $>0.2\,\mathrm{m\,s^{-1}}$. Figures 1a and 1c show values from the OFES model; Figures 1b and 1d are from the INALT01 model. Surface currents across the Agulhas Current near 30°E (indicated by filled circles in Figures 1a and 1b) were measured by Acoustic Doppler Current Profilers (ADCPs) on the Agulhas Current Time-Series (ACT) moorings. Values from historical current meters (CM) located within 1000 m of the bottom are indicated by large filled circles in Figures 1c and 1d, while small filled circles indicate values from current meters located more than 1000 m above the bottom. Vectors indicate simulated mean surface (Figures 1a and 1b) and bottom (Figures 1c and 1d) currents. Thick, medium, and thin solid contours represent isobaths of 1500, 3000, and 4500 m, respectively. Dashed lines highlight locations of the 18.2°E and 40.1°S sections shown in Figure 2.

2009], which is proportional to dissipation rate. The metric we consider is percentage of record with speeds greater than some threshold value, in this case $0.2\,\mathrm{m\,s^{-1}}$ for deep flows and $0.5\,\mathrm{m\,s^{-1}}$ for surface flows. This provides a simple measure of the prevalence of strong bottom currents and is an important metric for sediment transport and engineering design studies. Our choice of threshold values is somewhat arbitrary, being based on engineering tolerances for ocean-observing platforms.

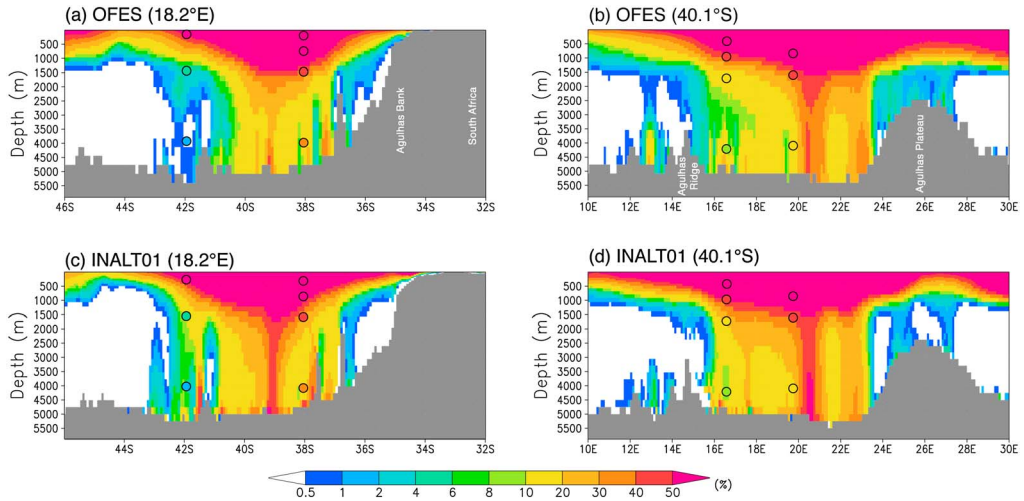

Figure 2. Cross-section along 18.2°E (left) and 40.1°S (right) of percentage of record with currents >0.2 m s^{-1} for OFES (top) and INALT01 (bottom). Filled circles show values from historical current meters located near sections (see Figure 1).

For example, a moored surface buoy (http://www.pmel.noaa.gov/OCS/ARC), recently deployed in the ARC, could tolerate strong surface currents but broke away from its anchor when this was combined with a deep current >0.3 m s^{-1}.

[6] Threshold bottom velocities are also used for determining sediment transport: Below a threshold shear, the lifting force is insufficient to dislodge noncohesive particles off the sediment bed, and likewise, suspended matter of this size and larger will be deposited. In particular, using a bottom drag coefficient value of 0.0025 (the value used in one of the models here), the 0.2 m s^{-1} threshold bottom velocity can be converted into a threshold frictional velocity, which, according to the *Miller et al.* [1977] Shield's diagram, is capable of lifting noncohesive quartz-density particles smaller than 70 µm. Consequently, particles smaller than 70 µm (e.g., very fine sand) are unlikely to be found in regions that frequently have benthic currents greater than 0.2 m s^{-1} and contourites [*Schlüter and Uenzelmann-Neben*, 2007] can be expected downstream in regions of decelerated flow.

[7] Because our primary objective is to document the existence of strong benthic flow, regardless of time scale or source, the analysis is performed on unfiltered current meter data and model output. The analysis uses recently recovered current meters from the Agulhas Current Time-Series (ACT) experiment (http://act.rsmas.miami.edu) and historic current meter data found in the WOCE Kepler database (http://kepler.oce.orst.edu). In particular, three data sets are used here: 5 ACT moorings, 10 moorings that were deployed in the Agulhas Retroflection region from 1985 to 1987 [*Luyten et al.*, 1990], and 5 moorings deployed, as part of WOCE SCM9, near the Prince Edward Islands just south of the ARC from 1993 to 1995 [*Read and Pollard*, 1999]. All moorings in the study domain were in water depth greater than 1500 m and had current meters 46–1325 m off the bottom. The five ACT moorings also included upward-looking Acoustic Doppler Current Profiler (ADCP) measurements from which surface currents could be inferred.

[8] Two high-resolution OGCMs are used in this analysis: the Japanese Ocean model For the Earth Simulator (OFES) [*Masumoto et al.*, 2004] and the German INALT01 (updated AG01) [*Biastoch et al.*, 2009] model. Both were run in hindcast mode under prescribed atmospheric forcing for multiple decades. OFES, based on the Modular Ocean Model (MOM3) [*Pacanowski and Griffies*, 1999], has horizontal grid spacing of 1/10° and 54 vertical levels varying from 5 m at the surface to up to 330 m at the bottom in the deepest regions of the nearly global domain. INALT01 is a nested configuration based on the NEMO code v3.1.1 [*Madec*, 2008]. It consists of a high-resolution 1/10° nest covering the western South Indian and the entire South Atlantic basins (8°N–50°S, 70°W–70°E) embedded in a two-way mode (AGRIF) [*Debreu et al.*, 2008] within a global ocean–sea ice 1/2° base model. Both the high-resolution and global components of the INALT01 model have 46 z levels and, like the OFES model, partially filled bottom cells. The partial cell method allows for more realistic horizontal pressure gradients associated with bottom topography [*Pacanowski and Gnanadesikan*, 1998] and, consequently, more realistic representation of flow associated with topography, such as topographic Rossby waves. Both OFES and INALT01 have model topography constructed from 1/30° bathymetry data sets, created by the OCCAM project at Southampton Oceanography Centre in the former case and ETOPO-2 in the latter.

[9] Simulated bottom currents were taken from the bottom cell of each OGCM. The bottom cell was up to 330 and 250 m thick for OFES and INALT01, respectively. Thus, neither OGCM resolved the benthic Ekman layer. Likewise, except for one current meter that was placed 46 m above the bottom, all current meter sensors were placed well above the benthic boundary layer (i.e., up to 1325 m above the bottom). Currents within 1000 m of the bottom are considered bottom currents, while those more than 1000 m above the bottom are considered deep currents. When the analysis was repeated using one or two bins above the bottom bin, the OGCM results were qualitatively unchanged. Bottom friction is estimated using a drag coefficient value of 0.0025 in OFES. While the INALT01 value is smaller, 0.001, it is applied to the squared bottom currents increased by a value of 0.0025 m^2 s^{-2} to account for bottom turbulent kinetic energy due to tides and other unresolved currents.

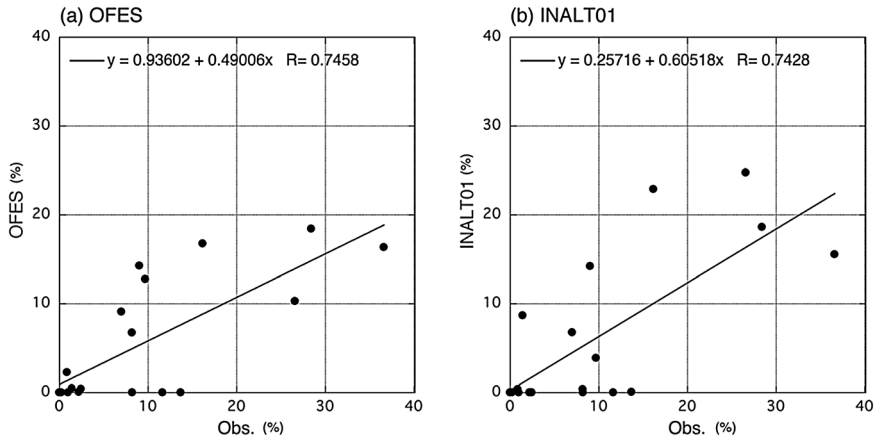

Figure 3. Scatter plot of percentage of record with observed versus simulated bottom currents >0.2 m/s from the (a) OFES and (b) INALT01 models. The overall cross-correlation between the observed and simulated values is 0.7 for both models.

[10] Neither model assimilated observations, which has been shown to improve simulations in the deep ocean [*Scott et al*., 2010]. OFES model was forced from 1950 to 2007 with daily mean fluxes derived from NCEP/NCAR reanalysis [*Kalnay et al*., 1996], and 3 day snapshots from 1980 to 2006 were used in the OFES analysis here. INALT01 was forced from 1948 to 2007 with CORE2b atmospheric forcing fields [*Large and Yeager*, 2009] at six-hourly resolution. Thus INALT01, to a certain extent, supports inertial oscillations and internal waves. Neither model, however, simulated tides, which could lead to higher bottom currents near seamounts and shallow topography.

3. Results

[11] Bottom currents exceed 0.2 m s^{-1} more than 50% of the time in narrow regions beneath the Agulhas Current and below the mean retroflection front, indicative of mean deep jets (Figure 1). The shelf region east of South Africa is moderately productive and thus has sediment enriched with organic and particulate carbon. Where these bottom jets flow off the continental shelf, we expect export of carbon into the abyss (see Figures S1 and S2). Benthic storms, with currents that exceed 0.2 m s^{-1}, occur 20% of the time in broad areas of the retroflection region and beneath the ARC (Figure 1). The slightly stronger bottom currents in INALT01 may be due to its smaller drag coefficient in regions of strong currents. To investigate the effects of missing tides and high-frequency forcing on bottom currents, we low-pass filtered the current meter data from the retroflection region and found that the values shown in Figure 1 were reduced by no more than 2%, suggesting that the peak bottom currents are relatively insensitive to inertial oscillations and tides.

[12] The position of the surface currents relative to these bottom currents can be seen in Figure 1, where the prevalence of surface currents greater than 0.5 m s^{-1} illustrates the path of the Agulhas Current, its retroflection, and the eastward flowing ARC. Away from the strong upper ocean currents, the deep ocean is quiescent, with bottom currents rarely or never exceeding 0.2 m s^{-1}, even close to topography. Curiously, bottom currents are very weak in a narrow (~50 km) band along the flanks of the Agulhas Plateau, even though the surface currents are intense (>0.5 m s^{-1} more than 50% of the time). This may be because the necessary conditions for baroclinic instability are not met due to the influence of sloping topography [*Gill et al*., 1974]. Northeast of the Agulhas Plateau, in the Transkei basin where the bottom currents converge into a region of relatively quiescent flow, contourites have been observed in the sedimentary record [*Schlüter and Uenzelmann-Neben*, 2007]. Favorable conditions for contourites can also be seen where the energetic bottom flow extends into the Cape Basin, and similarly where it abuts the southwest flank of the Agulhas Plateau. For regional details of Figures 1c and 1d, see Figures S1–S7.

[13] In general, currents are surface intensified. However, as shown in Figure 2, bottom intensified currents are common, particularly near seamounts and ridges [*Lavelle and Mohn*, 2010; *Bishop et al*., 2012]. Bottom intensification is not seen in the current meter records, probably due to the lack of vertical resolution on these moorings. Bottom intensification may also explain the discrepancy between the simulations and observations along 23°E in Figure 1: The current meters are located more than 1000 m above the bottom. However, even with these height discrepancies, the scatter between the observed values and the OGCM bottom bin values is modest, with a cross-correlation of 0.7 for both models (Figure 3).

4. Discussion and Conclusion

[14] The relatively good agreement between the two OGCMs and the current meter measurements lends confidence that our results are robust. In order to gain intuition about these benthic storms, we compare our results to a similar analysis of the prevalence of sea winds >20 m s^{-1} (Beaufort 9 strong gale force winds) [*Sampe and Xie*, 2007]. The wind analysis shows that strong gale force winds occur only 10–20% of the time in the Northern and Southern Hemisphere storm tracks during winter, much less frequently than the strong bottom currents in our analysis (Figure 1), suggesting that their 20 m s^{-1} wind threshold is more stringent than our threshold.

[15] The Rossby deformation radius for the atmosphere and ocean is L_{at}~1400 km and L_{oc}~30 km, respectively [*Bluestein*, 1992; *Chelton et al*., 1998]. Thus, for

comparable Rossby numbers (ratio of the inertial force to the Coriolis force), the oceanic and atmospheric velocities scale as $U_{at}/U_{oc} \sim L_{at}/L_{oc} \sim 1400\,\mathrm{km}/30\,\mathrm{km} \sim 47$. In other words, a $0.2\,\mathrm{m\,s^{-1}}$ benthic storm would be comparable to a $9\,\mathrm{m\,s^{-1}}$ (Beaufort 5) windstorm. However, a mere $5\,\mathrm{m\,s^{-1}}$ wind is sufficient to lift a 70 μm noncohesive particle (corresponding to the threshold benthic flow of $\sim 0.2\,\mathrm{m\,s^{-1}}$) [*Bagnold*, 1941; *Miller et al*., 1977]. Windstorms thus appear to be more effective than benthic storms at lifting noncohesive particles. This is due in part to the fact that a windstorm with the same Rossby number as the benthic storm will have a larger particle Reynold's number (UL_{part}/ν) due to the relative magnitudes of the atmospheric and oceanic molecular viscosities ($\nu_{at}/\nu_{oc} \sim 1.4 \times 10^{-5}\,\mathrm{m^2\,s^{-1}}/1.8 \times 10^{-6}\,\mathrm{m^2\,s^{-1}} \sim 8$). It should be noted that for a dust storm to form, the resulting lifting must be combined with large vertical motion and thus must have a large Rossby number, i.e., horizontal scales much smaller than the Rossby deformation radius. The effective viscosity may be much larger than the molecular viscosity, and other processes may play a role. An interesting follow-on study would be to compare the prevalence of thick nepheloid layers to thick dust storms.

[16] Our results show the prevalence of strong bottom currents beneath the Agulhas System surface currents, suggesting that in western boundary current regions, energy can be effectively transferred to the deep ocean where it is dissipated through friction, making these regions important in the global energy balance. *Arbic et al*. [2009] estimated that the global bottom drag dissipation rate is in the range of 0.14–0.65 TW and therefore represents a substantial sink for the 1 TW of wind power that is transformed into geostrophic motions. The linkage between benthic storms and surface currents, demonstrated here, leads to serious engineering design constraints for oceanic observing systems but points to the potential for sediment analyses to provide important clues not only to paleo-bottom currents but also to paleo-surface currents. We hope that this study will inspire further research on these dynamic and powerful deep currents.

[17] **Acknowledgment.** We thank G. Uenzelmann-Neben and an anonymous reviewer for their helpful comments. The OFES simulation was conducted on the Earth Simulator under the support of JAMSTEC. The development of INALT01 and its analysis received funding from the European Community's Seventh Framework Programme FP7/2007-2013—Marie-Curie ITN, under grant agreement n° 238512, GATEWAYS project. T.T. was supported by JST/JICA through Science and Technology Research Partnership for Sustainable Development (SATREPS). This is PMEL publication contribution 3928.

References

Arbic, B. K., J. F. Shriver, P. J. Hogan, H. E. Hurlburt, J. L. McClean, E. J. Metzger, R. B. Scott, A. Sen, O. M. Smedstad, and A. J. Wallcraft (2009), Estimates of bottom flows and bottom boundary layer dissipation of the oceanic general circulation from global high-resolution models, *J. Geophys. Res.*, *114*, C02024, doi:10.1029/2008JC005072.

Bagnold, R. A. (1941), The Physics of Blown Sand and Desert Dunes, Methuen and Co. Ltd., London.

Beal, L., and H. Bryden (1999), The velocity and vorticity structure of the Agulhas Current at 32°S, *J. Geophys. Res.*, *104*, 5151–5176, doi:10.1029/1998JC900056.

Beal, L. M., W. P. M. de Ruijter, A. Biastoch, R. Zahn, and SCOR/IAPSO/WCRP Working Group 136 (2011), On the role of the Agulhas System in Ocean Circulation and Climate, *Nature*, *472*, 429–436, doi:10.1038/nature09983.

Biastoch, A., L. Beal, T. G. D. Casal, and J. R. E. Lutjeharms (2009), Variability and coherence of the Agulhas Undercurrent in a high-resolution ocean general circulation model, *J. Phys. Oceanogr.*, *39*, 2417–2435.

Biastoch, A., C. W. Böning, and J. R. E. Lutjeharms (2008), Agulhas leakage dynamics affects decadal variability in Atlantic overturning circulation, *Nature*, *456*, 489–492, doi:10.1038/nature07426.

Bishop, S. P., D. R. Watts, J.-H. Park, and H. G. Hogg (2012), Evidence of bottom-trapped currents in the Kuroshio Extension region, *J. Phys. Oceanogr.*, *42*, 321–328.

Bluestein, H. B. (1992), *Synoptic-Dynamic Meteorology in Midlatitudes*, vol. 1, 431 pp., Oxford University Press, New York, NY.

Boebel, O., T. Rossby, J. Lutjeharms, W. Zenk, and C. Barron (2003), Path and variability of the Agulhas Return Current, *Deep Sea Res., Part II*, *50*, 35–56.

Chelton, D. B., R. A. deSzoeke, M. G. Schlax, K. E. Naggar, and N. Siwertz (1998), Geographical variability of the first baroclinic Rossby radius of deformation, *J. Phys. Oceanogr.*, *28*, 433–460.

Chereskin, T. K., K. A. Donohue, D. R. Watts, K. L. Tracey, Y. L. Firing, and A. L. Cutting (2009), Strong bottom currents and cyclogenesis in Drake Passage, *Geophys. Res. Lett.*, *36*, L23602, doi:10.1029/2009GL040940.

Cronin, M. F., and D. R. Watts (1996), Eddy-mean flow interaction in the Gulf Stream at 68°W: Part I. Eddy energetics, *J. Phys. Oceanogr.*, *26*, 2107–2131.

Debreu, L., C. Vouland, and E. Blayo (2008), AGRIF: Adaptive grid refinement in Fortran, *Comput. Geosci.*, *34*, 8–13.

Ferrari, R., and C. Wunsch (2009), Ocean circulation kinetic energy—Reservoirs, sources and sinks, *Annu. Rev. Fluid Mech.*, *41*, 253–282.

Garzoli, S. L., et al. (2010), Progressing towards global sustained deep ocean observations, in *Proceedings of OceanObs'09: Sustained Ocean Observations and Information for Society (Vol. 2), Venice, Italy, 21–25 September 2009*, edited by J. Hall, D.E. Harrison and D. Stammer, ESA Publication WPP-306, doi:10.5270/OceanObs09.cwp.34

Gill, A. E., J. S. A. Green, and A. J. Simmons (1974), Energy partition in the large-scale ocean circulation and the production of mid-ocean eddies, *Deep Sea Res.*, *21*, 499–528.

Hogg, N. (1983), A note on the deep circulation of the western North Atlantic: Its nature and causes, *Deep Sea Res.*, *30*, 945–961.

Kalnay, E., et al. (1996), The NCEP/NCAR 40-year reanalysis project, *Bull. Am. Meteorol. Soc.*, *77*, 437–470.

Kontar, E. A., and A. V. Sokov (1997), On the benthic boundary layer's dynamics, *J. Mar. Syst.*, *11*, 369–385.

Large, W. G., and S. G. Yeager (2009), The global climatology of an interannually varying air-sea flux data set, *Clim. Dyn.*, *33*, 341–364, doi:10.1007/s00382-008-0441-3.

Lavelle, J. W., and C. Mohn (2010), Motion, commotion, and biophysical connections at deep ocean seamounts, *Oceanography*, *23*, 90–103, http://dx.doi.org/10.5670/oceanog.2010.64.

Luyten, J., et al. (1990), Moored current meter, AVHRR, CTD, and drifter data from the Agulhas Current and Retroflexion region (1985–1987), Vol. 42, XLII, *Woods Hole Oceanographic Institution Tech. Rep., WHOI-90-30*, 100 pp.

Madec, G. (2008), NEMO ocean engine, Note du Pole de modélisation, Institut Pierre-Simon Laplace (IPSL), France.

Masumoto, Y., et al. (2004), A fifty-year eddy-resolving simulation of the world ocean—Preliminary outcomes of OFES (OGCM for the Earth Simulator), *J. Earth Simul.*, *1*, 35–56.

Miller, M. C., I. N. McCave, and P. D. Komar (1977), Threshold of sediment motion under unidirectional currents, *Sedimentology*, *24*, 507–527.

Pacanowski, R. C., and A. Gnanadesikan (1998), Transit response in a *z*-level ocean model that resolves topography with partial-cells, *Mon. Weather Rev.*, *126*, 3248–3270.

Pacanowski, R. C., and S. M. Griffies (1999), MOM 3.0 manual, *GFDL Ocean Group Tech Rep. 4*, NOAA/GFDL, Princeton, NJ, 680 pp.

Park, J.-H., K. A. Donohue, D. R. Watts, and L. Rainville (2010), Distribution of deep near-inertial waves observed in the Kuroshio Extension, *J. Oceanogr.*, *66*, 709–717.

Read, J. F., and R. T. Pollard (1999), Deep inflow into the Mozambique Basin, *J. Geophys. Res.*, *104*, 3075–3090, doi:10.1029/1998JC900078.

Sampe, T., and S.-P. Xie (2007), Mapping high sea winds from space: A global climatology, *Bull. Am. Meteorol. Soc.*, *88*, 1965–1978.

Savidge, D. K., and J. M. Bane Jr. (1999), Cyclogenesis in the deep ocean beneath the Gulf Stream: 1. Description, *J. Geophys. Res.*, *104*, 18,111–18,126, doi:10.1029/1999JC900132.

Schlüter, P., and G. Uenzelmann-Neben (2007), Seismostratigraphic analysis of the Transkei Basin: A history of deep sea current controlled sedimentation, *Mar. Geol.*, *240*, 99–111.

Scott, R. B., et al. (2010), Total kinetic energy in four global eddying ocean circulation models and over 5000 current meter records, *Ocean Modell.*, *32*, 157–169, doi:10.1016/j.ocemod.2010.01.005.

Thompson, R., and J. R. Luyten (1976), Evidence for bottom trapped topographic Rossby waves from single moorings, *Deep Sea Res.*, *23*, 629–635.

Zahn, R., J. Lutjeharms, A. Biastoch, I. Hall, G. Knorr, W. Park, and C. Reason (2010), Investigating the Global Impacts of the Agulhas Current, *Eos Trans. AGU*, *91*(12), 109, doi:10.1029/2010EO120001.